APPENDIX

APPENDIX FIGURES S1−S12

LEGENDS TO APPENDIX FIGURES S1−S12

APPENDIX REFERENCES

Mizuta et al., Appendix Figure S1

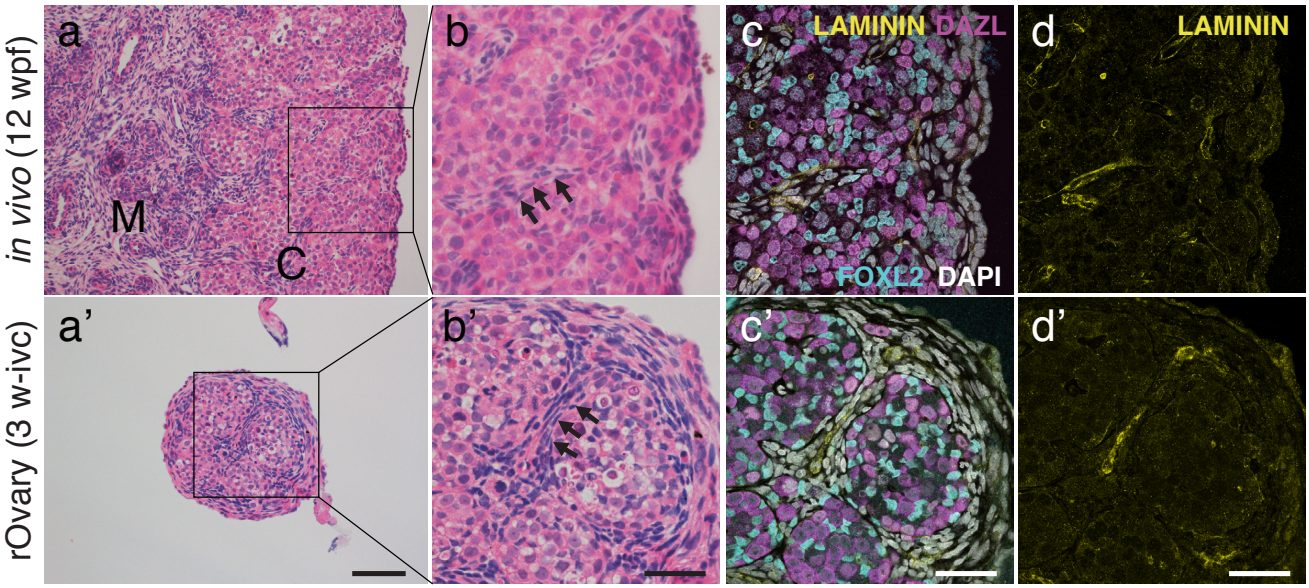

Mizuta et al., Appendix Figure S2

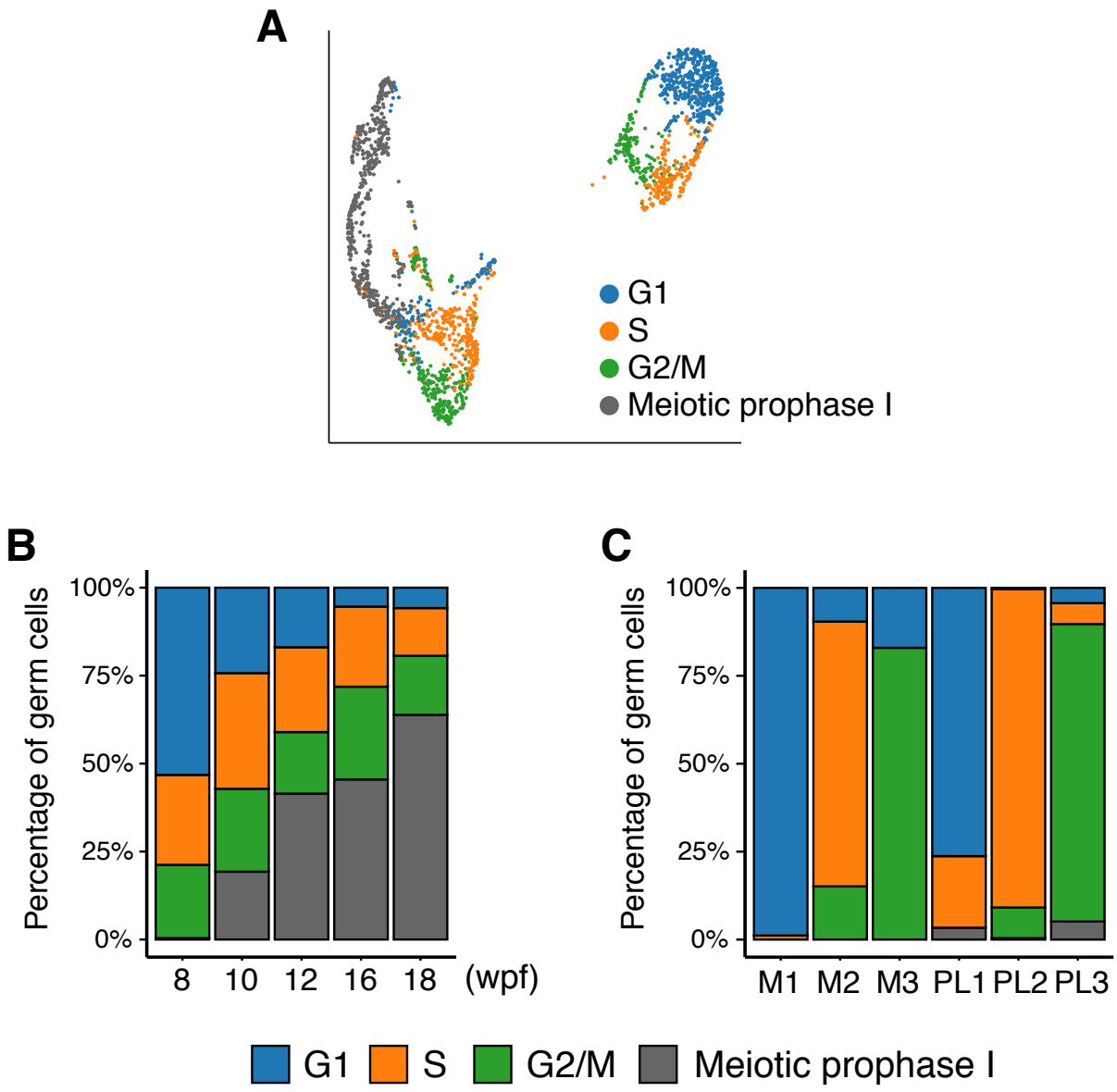

Mizuta et al., Appendix Figure S3

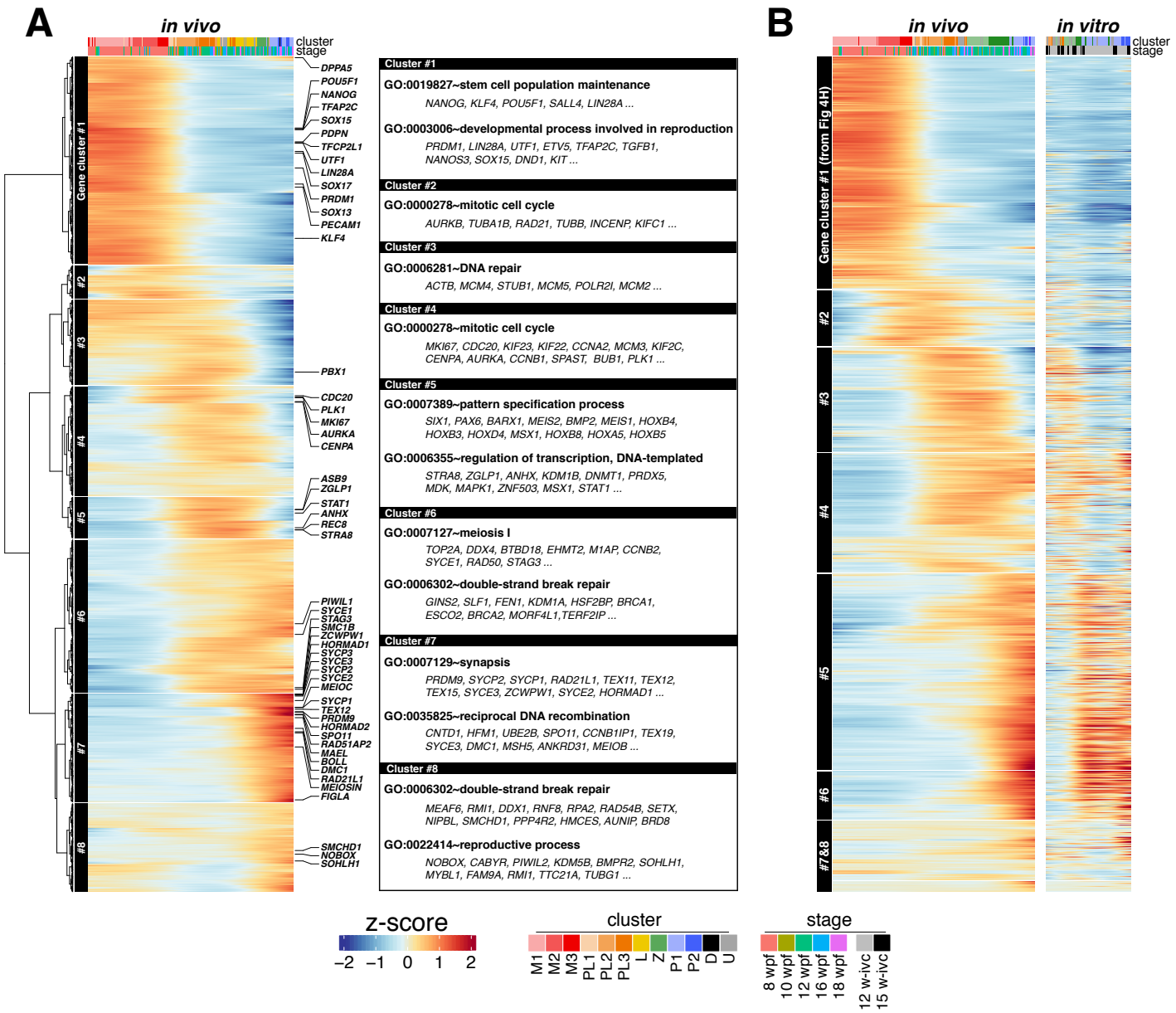

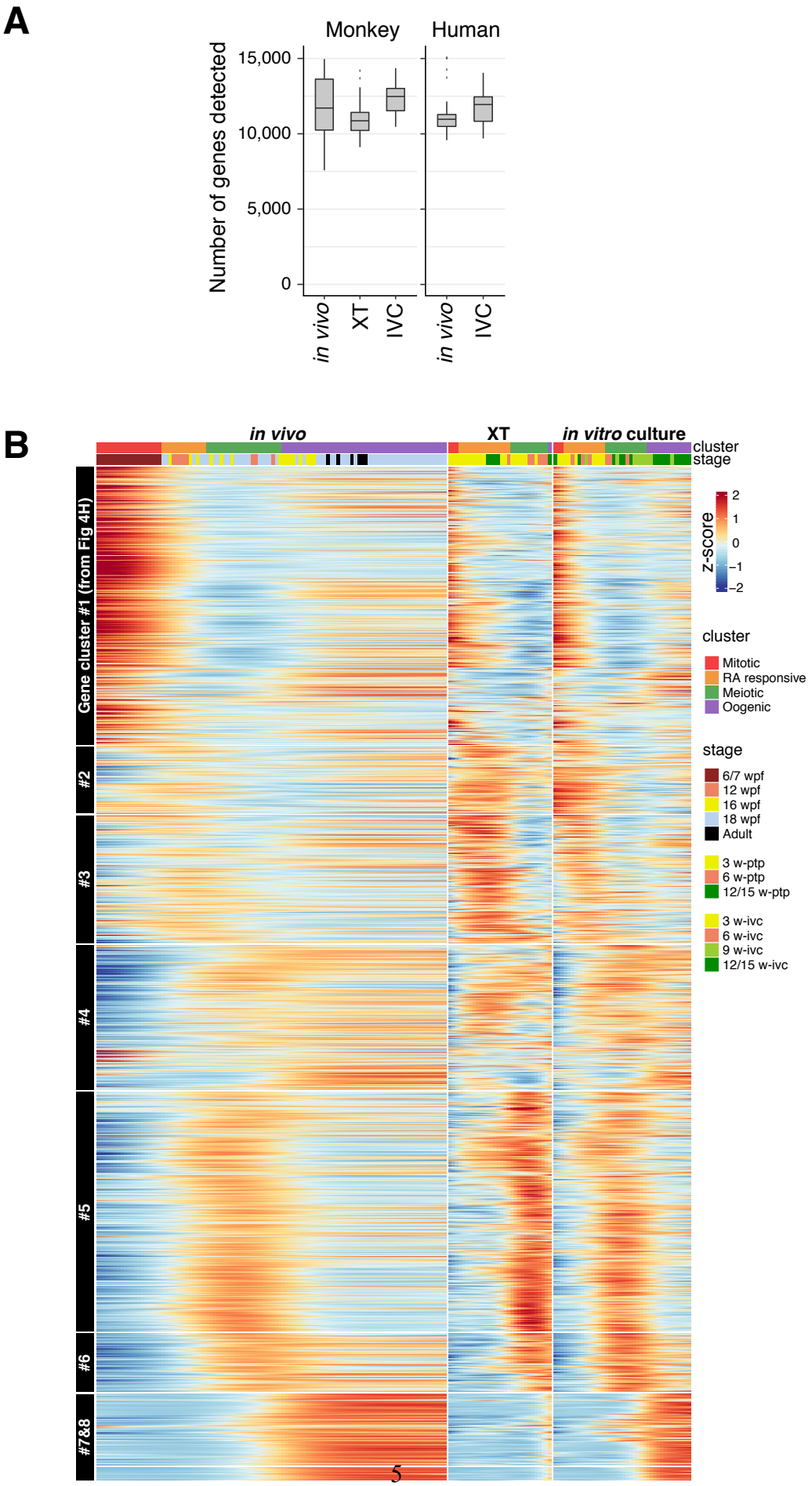
A
Monkey
Human
Number of genes detected
15,000
10,000
5,000
0
in vivo
XT
IVC
in vivo
IVC
B
in vivo
XT
in vitro culture
cluster
stage
Gene cluster #1 (from Fig 4H)
#2
#3
#4
#5
#6
#7&8
z-score
2
1
0
−1
−2
cluster
Mitotic
RA responsive
Meiotic
Oogenic
stage
6/7 wpf
12 wpf
16 wpf
18 wpf
Adult
3 w-ptp
6 w-ptp
12/15 w-ptp
3 w-ivc
6 w-ivc
9 w-ivc
12/15 w-ivc

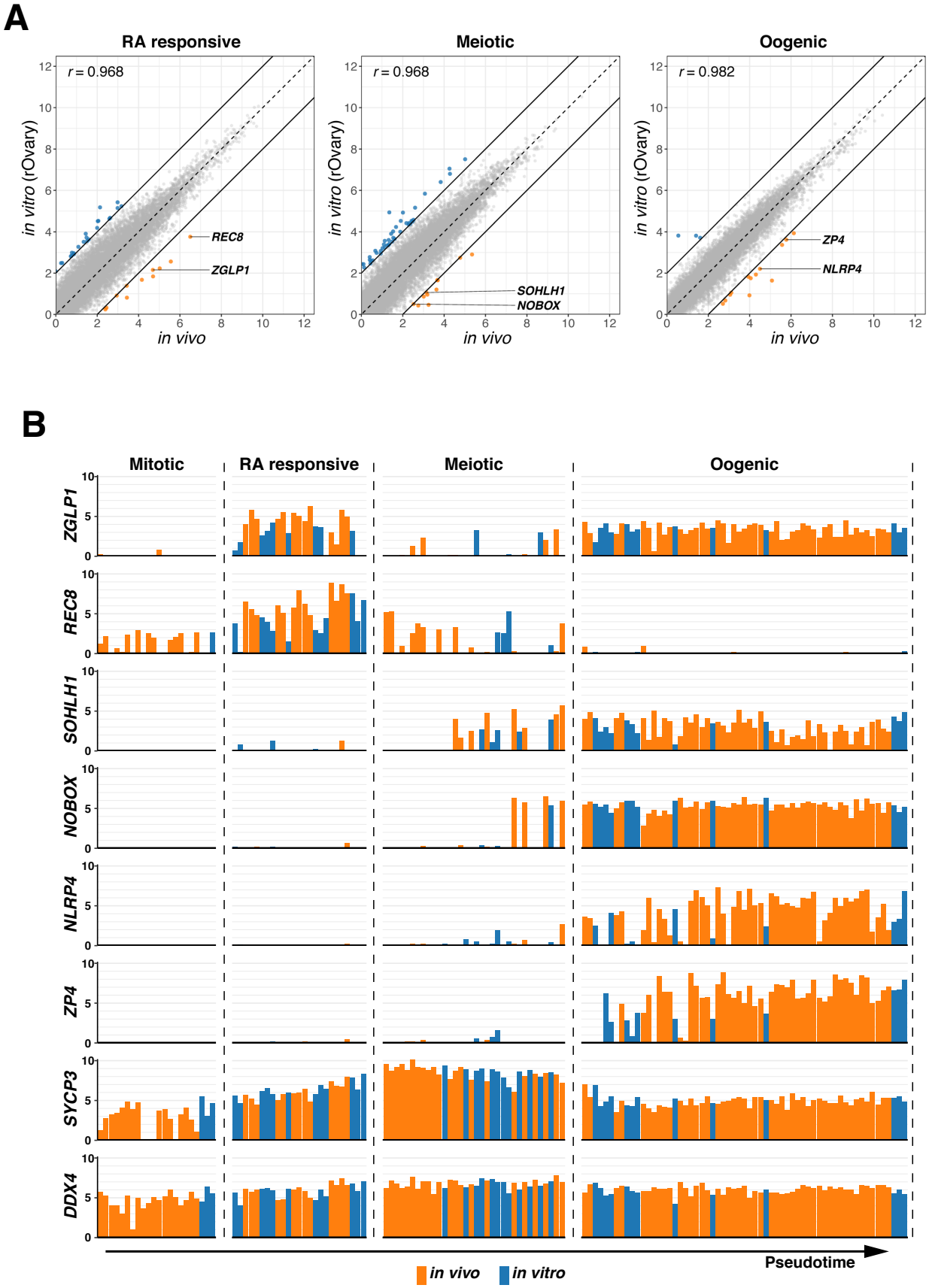
A
RA responsive
Meiotic
Oogenic
r = 0.968
r = 0.968
r = 0.982
in vitro (rOvary)
in vivo
REC8
ZGLP1
SOHLH1
NOBOX
ZP4
NLRP4
B
Mitotic
RA responsive
Meiotic
Oogenic
ZGLP1
REC8
SOHLH1
NOBOX
NLRP4
ZP4
SYCP3
DDX4
Pseudotime
in vivo
in vitro

Mizuta et al., Appendix Figure S6

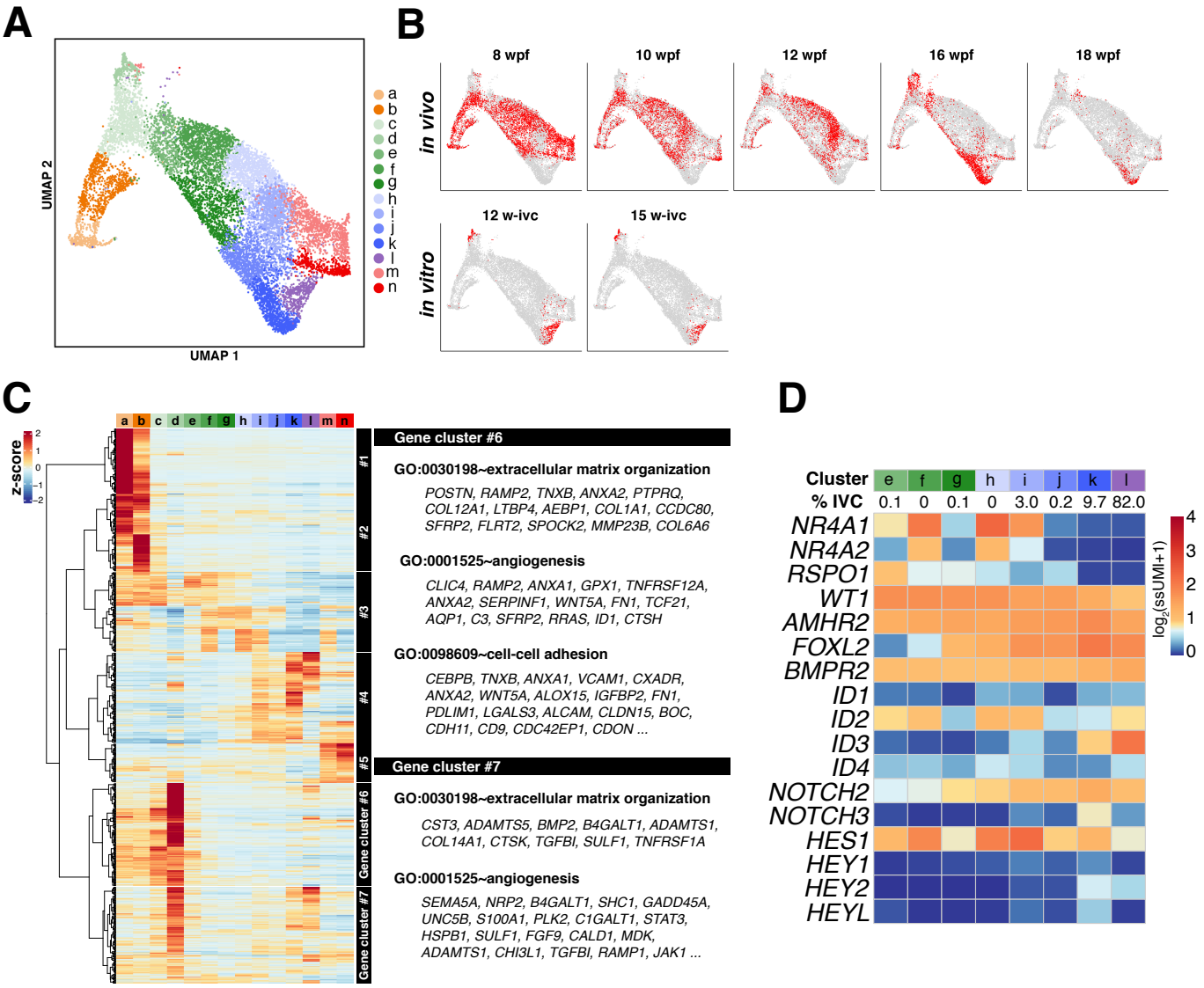

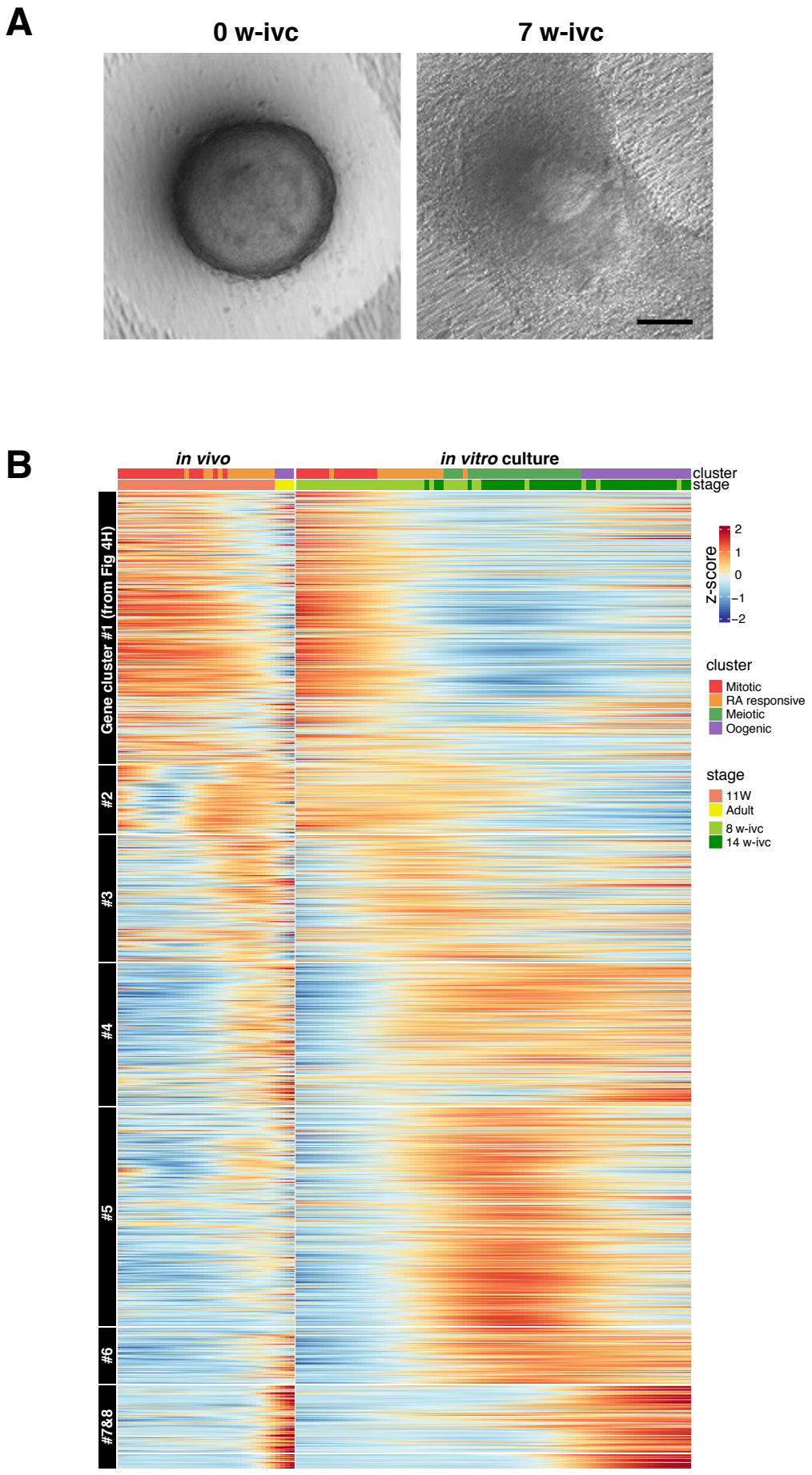
A
0 w-ivc
7 w-ivc
B
in vivo
in vitro culture
cluster
stage
Gene cluster #1 (from Fig 4H)
#2
#3
#4
#5
#6
#7&8
z-score
2
1
0
−1
−2
cluster
Mitotic
RA responsive
Meiotic
Oogenic
stage
11W
Adult
8 w-ivc
14 w-ivc

Mizuta et al., Appendix Figure S8

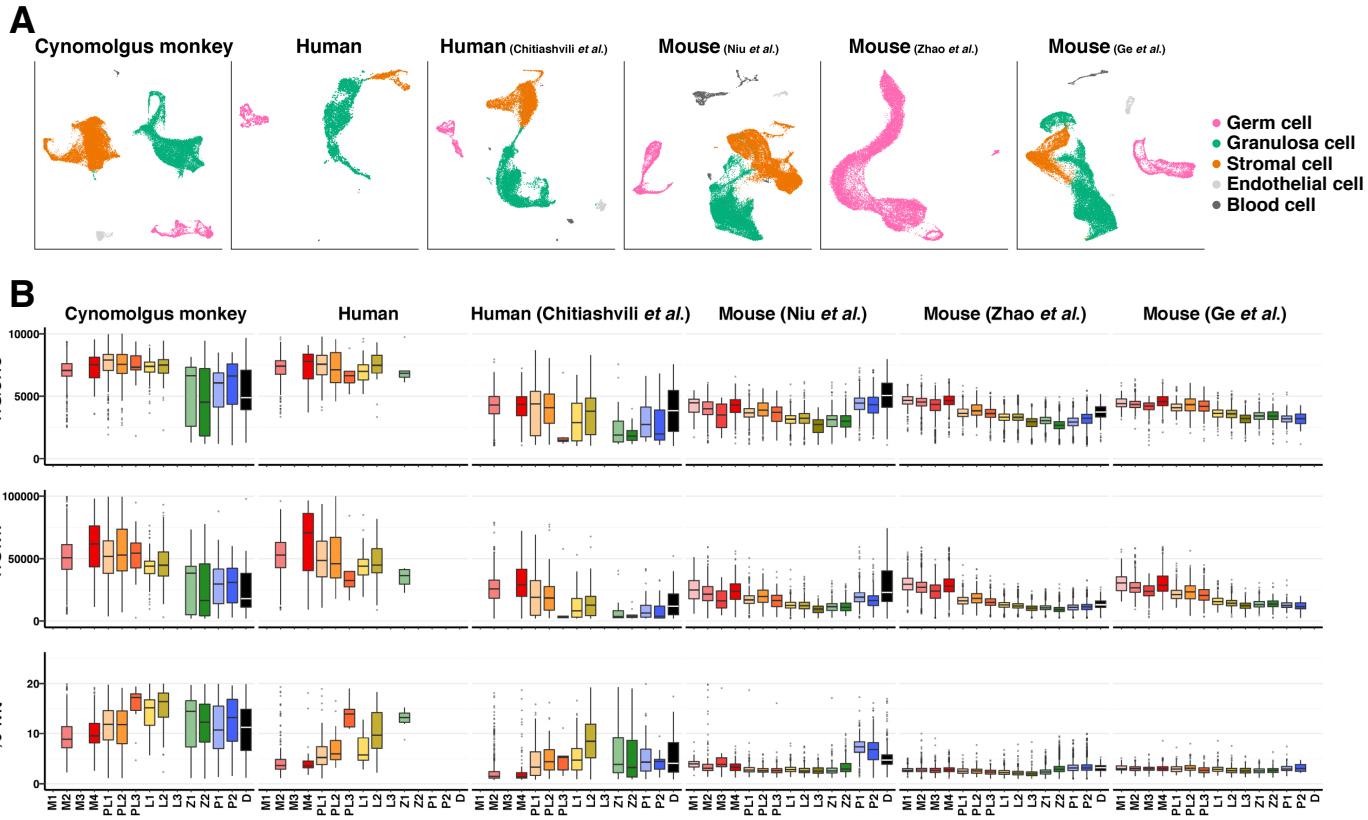

Mizuta et al., Appendix Figure S9

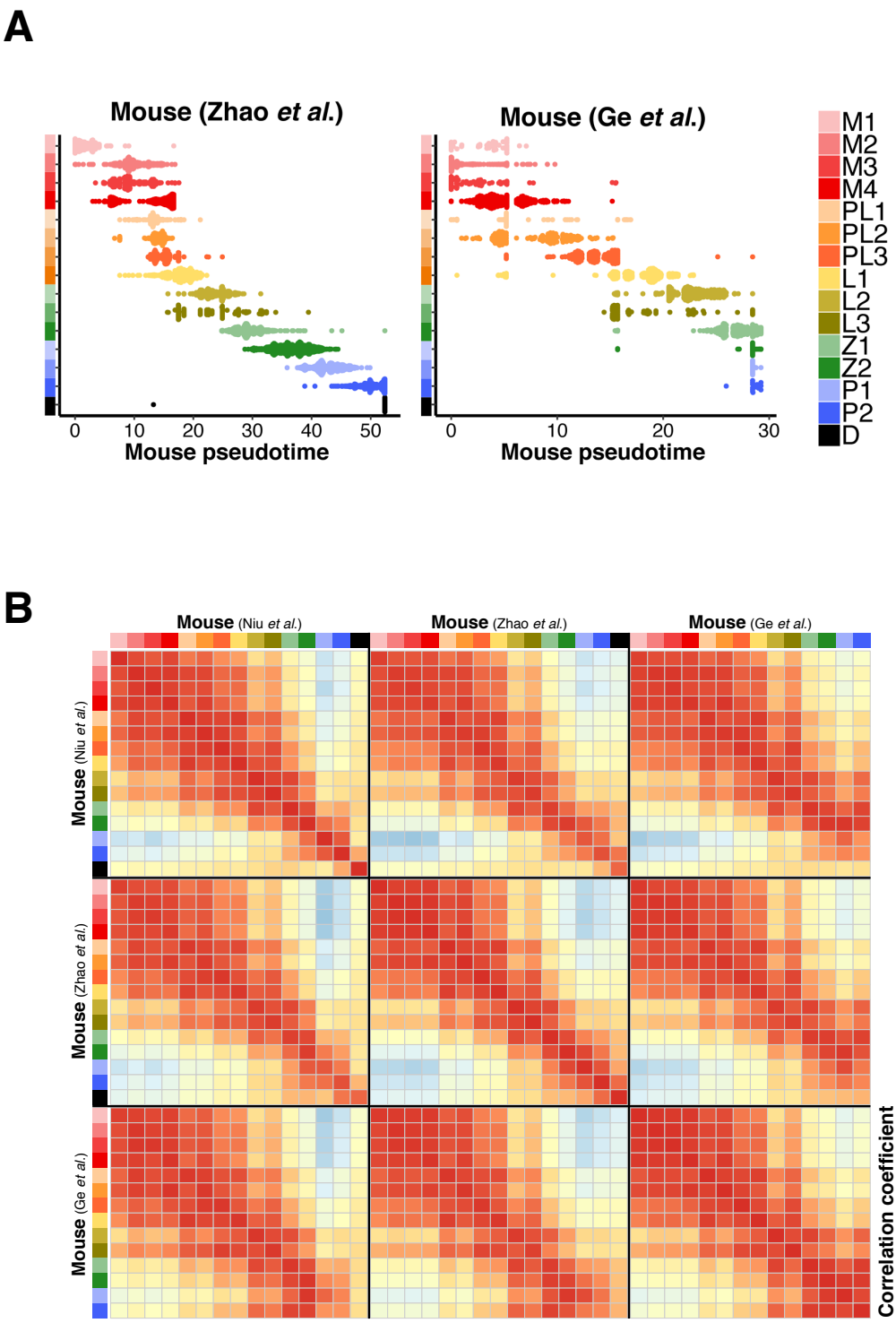

Mizuta et al., Appendix Figure S10

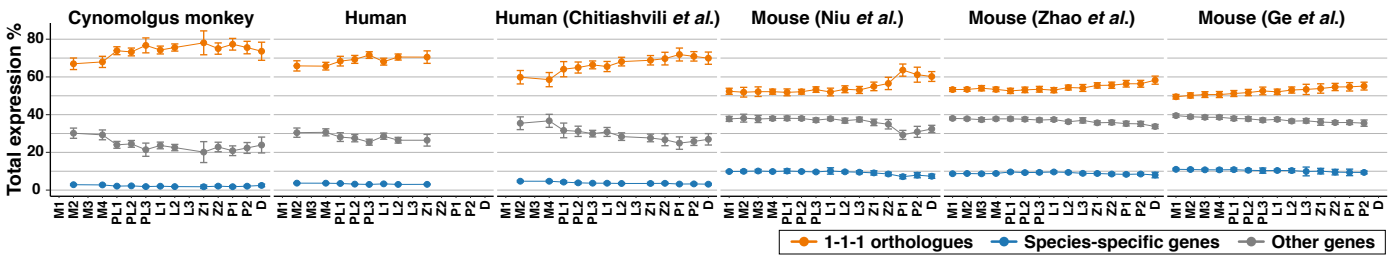

Mizuta et al., Appendix Figure S11

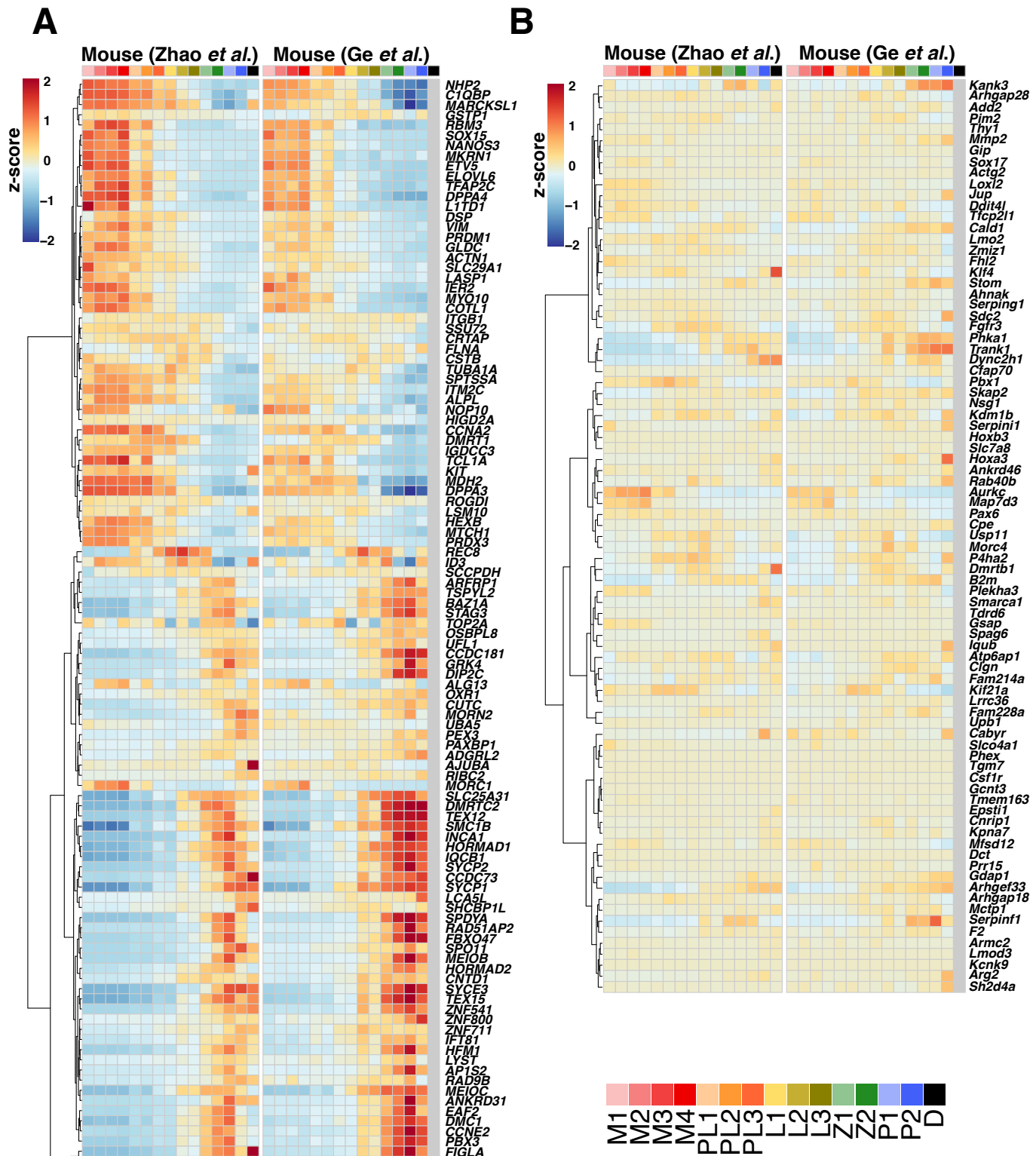

Mizuta et al., Appendix Figure S12

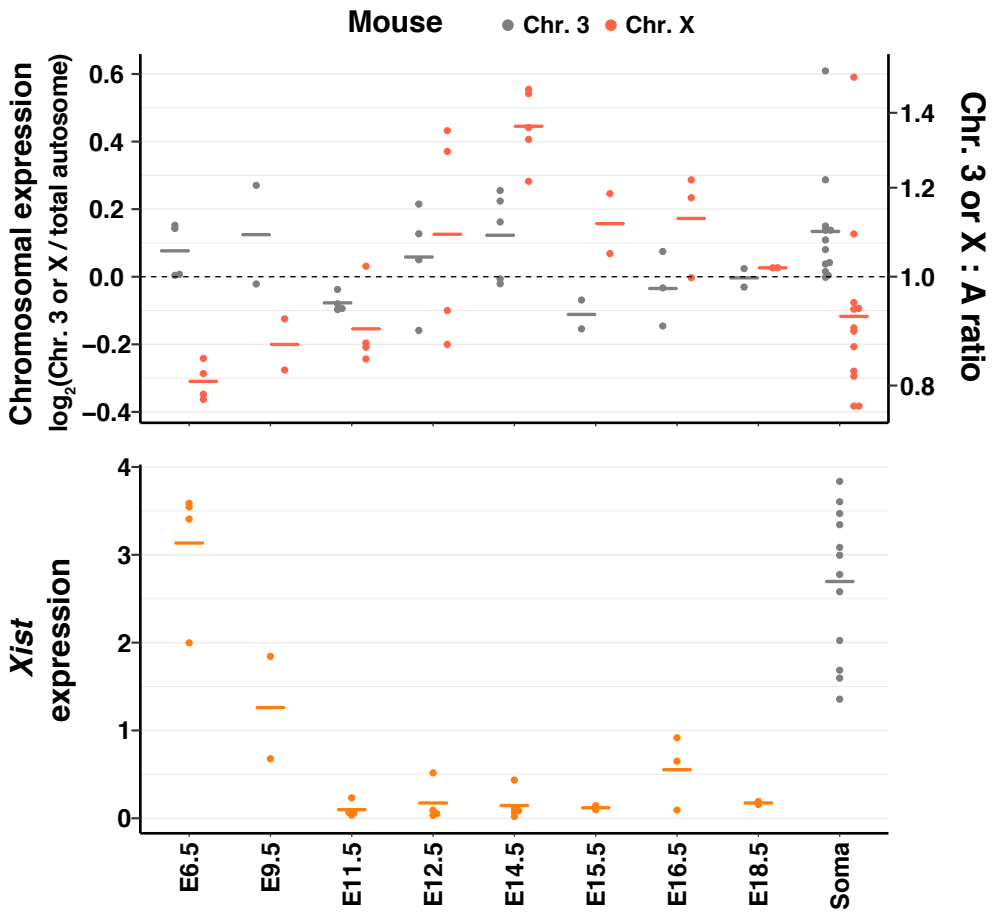

LEGENDS TO APPENDIX FIGURES

Appendix Figure S1. Reconstruction of the local structure of the ovarian cortex in cy rOvaries.

H&E staining (a and b) and IF for LAMININ/FOXL2/DAZL/DAPI (c and d) of a cy *in vivo* ovary (12 wpf) and cultured cy rOvary (3 w-ivc). Arrows indicate interstitial cells with a densely stained nucleus and a large nuclear-cytoplasmic ratio composing the cord-like structure. LAMININ, basement membrane marker; FOXL2, granulosa cell marker; DAZL, germ cell marker; DAPI, nucleus. M, medulla; C, cortex. Scale bars = 100 μm (a) and 50 μm (b–d).

Appendix Figure S2. Cell-cycle phase scoring on the 10X scRNA-seq data for cy germ cells *in vivo*.

(A) The UMAP plot in Fig 4D, highlighting the cells for each cell-cycle stage, i.e., G1, S, G2/M, and meiotic prophase I. (B and C) Percentages of germ cells assigned to each cell-cycle stage. The X-axes indicate the cy fetal stage (B) and the germ-cell developmental stage (C). The color-codings are as indicated. M, mitotic; PL, pre-leptotene; L, leptotene.

Appendix Figure S3. The pseudo-temporal expression patterns of HVGs with the 10X scRNA-seq datasets.

(A) (Left) Heatmap of highly variable genes (HVGs) along the pseudo-time trajectory (shown in Fig 4G) for cy germ cells *in vivo*. The HVGs [2,924 genes; Moran's $I > 0.2$ and q-value < 0.01] were identified across the trajectory based on the Moran's *I* statistic using Monocle 3. Eight gene clusters were defined according to the UHC dendrogram. (Right) Representative genes and key gene ontology (GO) enrichments are shown. (B) Heatmap of the HVGs defined in Fig 4H along the pseudo-time trajectory for cy germ cells *in vivo* and *in vitro* (shown in Fig 4Jc). The color-coding is as indicated. M, mitotic; PL, pre-leptotene; L, leptotene; Z, zygotene; P, pachytene; D, diplotene; U, unclassified.

Appendix Figure S4. The quality of the SC3-seq analysis and the pseudo-temporal expression patterns of HVGs with the cy datasets.

(A) The numbers of genes detected by the SC3-seq analyses in cy/human oocytes from *in vivo* ovaries, xenotransplanted rOvaries, and *in vitro* rOvaries.

(B) Heatmap of the HVGs defined in Fig 4H along the SC3-seq pseudo-time trajectory for cy germ cells from *in vivo*, xenotransplanted rOvaries (XT), and *in vitro* cultured rOvaries (IVC). The color-coding is as indicated.

Appendix Figure S5. Comparison of the gene expression of cy fetal oocytes *in vivo* and *in vitro*.

(A) Scatter-plot comparisons of the averaged gene-expression values measured by SC3-

seq between *in vivo* and *in vitro* RA-responsive (left), meiotic (middle), and oogenic (right) cells. The differentially expressed genes (DEGs) were defined as those showing a more than 4-fold difference (continuous diagonal lines) in expression (Nakamura, Yabuta et al., 2015). The genes defined as up-regulated *in vivo* and *in vitro* were colored in orange and blue, respectively. The X and Y axes indicate the $\log_2$(normalized read counts+1) expression values. *r* value, Pearson correlation coefficient. (B) Bar graphs showing the expression levels of key genes for oocyte development detected as DEGs in Appendix Fig S5A. Cells *in vivo* and *in vitro* were arranged along the pseudo-time trajectory. The color coding is as indicated.

Appendix Figure S6. 10X scRNA-seq analysis for cy granulosa cells *in vivo* and in rOvaries.

(A) UMAP plot for granulosa cells from cy *in vivo* fetal ovaries and *in vitro* cultured cy rOvaries, shown with the granulosa sub-clusters, i.e., clusters a–n. The color-coding is as indicated. (B) The UMAP plot shown in Appendix Fig S6A, highlighting the cells for each developmental stage or *in vitro* culture period. (C) (Left) Heatmap of the standardized expression of HVGs (829 genes) among the sub-clusters ordered by UHC; eight gene clusters were defined according to the UHC dendrogram. (Right) Representative genes and key GO enrichments for clusters #6/7 are shown. (D) Heatmap of the average expression levels of granulosa cell marker, BMP signaling pathway (*BMPR2* and *ID1*/*2*/*3*/*4*), and NOTCH signaling pathway (*NOTCH2*/*3*, *HES1*, and *HEY1*/*2*/*L*) genes in granulosa cell sub-clusters e–l defined in Appendix Fig S6A. The percentages of cells derived from cultured rOvaries in each sub-cluster are shown (%IVC). The color-coding is as indicated.

Appendix Figure S7. Human rOvaries cultured under the air-liquid interface condition and the pseudo-temporal expression patterns of HVGs with the human SC3-seq datasets.

(A) Representative images of human rOvaries cultured on Transwell-COL membranes at 0 and 7 w-ivc. Scale bar = 200 μm.

(B) Heatmap of the orthologous HVGs in Fig 4H along the SC3-seq pseudo-time trajectory for human germ cells from *in vivo* and *in vitro* cultured rOvaries (IVC). The color-coding is as indicated.

Appendix Figure S8. Cross-species comparison of *in vivo* fetal oocyte development in humans, monkeys, and mice.

(A) UMAP plots of fetal ovarian cells in each 10X scRNA-seq dataset, colored by five computationally assigned major clusters based on the expression of cell-type-specific markers. (B) The detected gene number (nGene), UMI count (nUMI), and percentage of mitochondrial genes (%Mt) in each mitotic/meiotic sub-stage of six 10X scRNA-seq datasets. M, mitotic; PL, pre-leptotene; L, leptotene; Z, zygotene; P, pachytene; D,

diplotene.

Appendix Figure S9. Cross-species comparison using the two additional mouse 10X scRNA-seq datasets (Zhao *et al.* and Ge *et al.*).
(A) The distribution of germ cells along the individually calculated mouse-specific pseudo-time trajectories. The color-coding for the germ-cell stage is as indicated. M, mitotic; PL, pre-leptotene; L, leptotene; Z, zygotene; P, pachytene; D, diplotene. (B) Heatmap of the Pearson correlation coefficients of the average expression levels of 237 HVGs (1-1-1 orthologues) among the meiotic sub-stages in the three mouse datasets (Ge, Wang et al., 2021, Niu & Spradling, 2020, Zhao, Ma et al., 2020) (see **Materials and Methods**). The color-coding for the germ cell stage is as indicated in Appendix Fig S8A. The 'Mouse (Niu *et al.*)' vs. 'Mouse (Niu *et al.*)' part is the redisplay of Fig 6E.

Appendix Figure S10. Gene expression dynamics of 1-1-1 orthologues and species-specific genes in humans, monkeys, and mice.
The percentages of the average expression of gene classes (1-1-1 orthologues, species-specific, and other genes) during *in vivo* fetal oocyte development in humans, monkeys, and mice are shown with SDs. The color-coding is as indicated. M, mitotic; PL, pre-leptotene; L, leptotene; Z, zygotene; P, pachytene; D, diplotene.

Appendix Figure S11. The expression levels of conserved and primate-specific genes in **the two additional mouse 10X scRNA-seq datasets (Zhao *et al.* and Ge *et al.*).**
Heatmap of the standardized expression levels of the 130 genes conserved among the three species in Fig EV5A (A) and the 83 genes showing specific expression changes in humans and monkeys in Fig 6F (B) for the two mouse 10X datasets (Ge et al., 2021, Zhao et al., 2020). The color-coding for the germ-cell stage is as indicated.

Appendix Figure S12. Re-analysis of the Sangrithi *et al.* mouse RNA-seq dataset.
The bulk RNA-seq dataset for female (XX) embryonic germ cells from the study of Sangrtithi *et al*. (Sangrithi, Royo et al., 2017) was reanalyzed with the bioinformatics pipeline used for the analysis of our mouse bulk RNA-seq dataset (see **Materials and Methods**). The Chr.3:A and X:A ratios (top), and the *Xist* expression levels (bottom) were analyzed. Gonadal somatic cells at E14.5−18.5 were used for the comparison with the data in Fig 7A. Dots, individual data points; bar, mean. E, embryonic day; P, postnatal day; Soma, gonadal somatic cells.

APPENDIX REFERENCES

Ge W, Wang JJ, Zhang RQ, Tan SJ, Zhang FL, Liu WX, Li L, Sun XF, Cheng SF, Dyce PW, De Felici M, Shen W (2021) Dissecting the initiation of female meiosis in the mouse at single-cell resolution. Cell Mol Life Sci 78: 695-713

Nakamura T, Yabuta Y, Okamoto I, Aramaki S, Yokobayashi S, Kurimoto K, Sekiguchi K, Nakagawa M, Yamamoto T, Saitou M (2015) SC3-seq: a method for highly parallel and quantitative measurement of single-cell gene expression. Nucleic Acids Res 43: e60

Niu W, Spradling AC (2020) Two distinct pathways of pregranulosa cell differentiation support follicle formation in the mouse ovary. Proc Natl Acad Sci U S A 117: 20015-20026

Sangrithi MN, Royo H, Mahadevaiah SK, Ojarikre O, Bhaw L, Sesay A, Peters AH, Stadler M, Turner JM (2017) Non-Canonical and Sexually Dimorphic X Dosage Compensation States in the Mouse and Human Germline. Dev Cell 40: 289-301 e3

Zhao ZH, Ma JY, Meng TG, Wang ZB, Yue W, Zhou Q, Li S, Feng X, Hou Y, Schatten H, Ou XH, Sun QY (2020) Single-cell RNA sequencing reveals the landscape of early female germ cell development. FASEB J 34: 12634-12645